Muonium Formation as a Probe of Radiation Chemistry in Sub- and Supercritical Carbon Dioxide

Khashayar Ghandi,* Michael D. Bridges, Donald J. Arseneau, and Donald G. Fleming

Department of Chemistry and TRIUMF, University of British Columbia, Vancouver, British Columbia, Canada V6T 1Z1

Received: August 25, 2004; In Final Form: October 16, 2004

Muonium ($Mu = \mu^+e^-$), which can be considered a light isotope of the H atom, has been observed for the first time in supercritical CO_2 ($ScCO_2$). It is unreactive on a time scale of a few microseconds and over a wide density range from well below to well above the CO_2 critical density $\rho_c = 0.47$ g/cm^3. The fraction of muon polarization in muonium, P_{Mu}, does not vary significantly at low densities but changes quickly at the highest densities, approaching zero. This density dependence is reflected in a concomitant increase observed in the lost fraction of polarization, P_L, demonstrating that the dynamics of Mu formation and depolarization in $ScCO_2$ is a direct probe of radiolysis effects in the terminal muon radiation track. In marked contrast to previous studies in hydrogen-containing solvents, C_2H_6 and H_2O, over comparable density ranges, the diamagnetic fraction, P_D, was found to be almost independent of density in CO_2, attributed to the formation of the stable solvated $MuCO_2^+$ molecular ion in this hydrogen-free solvent. The differing density dependences of both the Mu and the diamagnetic fraction in CO_2, in comparison with the rather similar trends seen for both in C_2H_6 and H_2O, supports previous claims of a significant role played by proton (muon) transfer reactions in the competing processes involved in Mu formation in hydrogen-containing solvents. In addition to this being the first report of radiolysis effects accompanying energetic positive muons stopping in $ScCO_2$, it is the only report of end of track effects in this solvent, which has many applications in nuclear waste management and green chemistry. With a mass intermediate between that of the electron, which has provided most radiation−chemistry studies in $ScCO_2$ to date, and the proton (or alpha-particle), implanted muons provide a unique data set, characteristic of higher LET radiation, that may be relevant to radiolysis effects induced in $ScCO_2$ by alpha decay from heavy nuclei, for which there are no comparable studies.

1. Introduction

A supercritical fluid is any substance above its critical temperature and pressure, giving rise to only one equilibrium state of the system that combines the properties of both gases and liquids.[1−3] Recently, it has been demonstrated that μSR techniques can provide significant and unique information on radiation and transient chemistry in sub- and supercritical fluids, namely, in supercritical water.[4,5] To extend such studies to another green solvent, supercritical carbon dioxide ($ScCO_2$), with a critical point 31 °C, 73 atm, which offers a range of unusual applications in synthetic and industrial chemistry,[1−3,6] in waste management applications,[7−9] and in the development of $ScCO_2$ Brayton cycles in nuclear reactors,[10] we have undertaken a project to probe the radiation and transient chemistry of positive muons (μ^+) and muonium ($Mu = \mu^+e^-$) in $ScCO_2$.

Very little is known about the structure and dynamics of tracks produced by radiolysis under sub- and supercritical CO_2 conditions since there is no previous information on end-of-track radiolysis effects in $ScCO_2$. Hence, there is a need for forefront research on ionizing radiation-induced chemical processes in this medium. For example, to design efficient radiation-induced polymerization processes, information about the tuning of radiation effects in $ScCO_2$ would be desirable. There are only a few published papers on electron-induced radiation chemical processes in CO_2,[11−15] while there are no reports on any higher linear energy transfer (LET) radiation (LET is the average energy released per unit path length due to ionization and excitation processes[16]). Radiation−chemical processes due to higher LET radiation (e.g., in the case of α-particles from the radioactive decay of heavy nuclei in waste management applications)[7−9] can be expected to be very different from those of low LET electron radiation. To maximize the lifetime of materials used in the reaction vessels for the previous applications, and to minimize the transport of radioactive species, the chemistry involved in the radiolysis of $ScCO_2$ needs to be understood. Measurements on the chemistry involved in the radiolysis of $ScCO_2$ are difficult to carry out for higher LET radiation. The hostile conditions of high pressure and radiation are not well-suited to most chemical instrumentation, leading to a gap in our knowledge of higher LET processes in $ScCO_2$. The main purpose of the present paper is to explore the effects of ionizing radiation in $ScCO_2$ of a particle of intermediate mass, the positive muon, at comparable thermodynamic conditions to those used in radiation-induced polymerization and nuclear waste management studies, thereby helping to fill in this gap.

There are important differences in the thermalization processes of electrons and heavy charged particles in high-density fluids, affecting the LET and hence affecting the nature of the radiolysis process involved. The extent of solvent (here CO_2) decomposition due to ionizing radiation[16] is a strong function

* To whom correspondence should be addressed. E-mail: kghandi@triumf.ca. Tel.: (604) 519-0803.

10.1021/jp046166u CCC: $27.50
Published on Web 12/08/2004

of the absorbed energy density of the incident radiation, with higher LET radiation causing decomposition of the solvent medium, while low LET radiation leads to little or no decomposition. In low LET radiation, typified by fast electrons and ^{60}Co γ sources, transients are formed in small clusters or spurs on the order of 50 Å in diameter, which are themselves separated by distances on the order of 1000 Å.[16,17] The probability that a transient will escape from the spur before combining with another transient is, under these circumstances, relatively high. On the other hand, the high LET coefficient characteristic of alpha particles ensures that their spurs overlap to form what is effectively a track of closely spaced spurs,[16] facilitating inter-spur interactions as distances between spurs are reduced. Another difference between heavier ions and energetic electrons is that the latter come to rest primarily within their initial radiation spurs,[16,17] whereas the μ^+ (and α-particle) and its Mu-atom thermalizes further away from the initial spur; thus, the muon is a particularly sensitive probe of radiolysis effects at the end of a charged particle track.[18−26] Differing LETs and stopping distances give rise to distinct differences in measured yields of products and in escape yields of reactive radicals and ions.[16,17,26,27] Consequently, we anticipate that radiation chemistry effects, probed by stopping μ^+ in $ScCO_2$, will provide both unique and complementary information to that known from electron radiation, thereby furthering our knowledge of the effects of thermodynamic conditions on radiolysis processes involved in this increasingly important solvent.

In μSR, the initial spin polarization of the μ^+, at observation times, is distributed into three principal environments, depending on the nature of the stopping medium: diamagnetic, including molecules (like MuH, in water or hydrocarbons) and molecular ions (here CO_2Mu^+), with polarization P_D; paramagnetic muonium, with polarization P_{Mu}; and muoniated free-radicals, with polarization P_R[28] (here possibly, MuOCO). In the realm of radiation chemistry in supercritical fluids, it is important to be able to distinguish these different environments over a broad range of thermodynamic conditions, in real time, a distinct feature of the μSR technique, provided by measurement of their differing spin precession frequencies in a transverse magnetic field (TF).

In high-density fluid media, radiation chemistry and hot atom effects that might determine the primary distribution of muons into different species is expected to take place on a ps to sub-nanosecond time scale, thereby preserving the muon spin polarization.[18−26,28−30] Transformations among these species, including interactions with paramagnetic transients within the spurs and delayed Mu formation,[31,32] can lead to a loss of spin polarization, referred to as the lost or missing fraction, P_L, such that $P_D + P_{Mu} + P_R + P_L = 1$. It follows that studying the changing fractions of muon spin polarization with thermodynamic conditions allows one to pursue the dependency of temporal radiation-induced effects on the thermodynamic conditions in supercritical fluids.[25] It therefore serves as a unique probe of the mechanisms of inhomogeneous, nonequilibrium radiation chemistry process, here in $ScCO_2$ in particular. Since previous μSR studies of the density dependence of radiolysis effects and the measurements of polarization fractions as a function of density over a broad range have only been carried out in hydrogen-containing fluids,[25,33] the present study is unique in that it allows an interpretation of these fractions in comparison with those in a hydrogen-free solvent.

While Mu has been studied in solid CO_2, over a wide range of temperatures, from 10 to 200 K,[34] there has been no previous report of Mu formation in liquid, gas, or $ScCO_2$. Moreover, the principal focus of ref 34 was a measurement of muonium spin relaxation rates in the solid CO_2 lattice. An important aspect of the current study is to measure, for the first time, these fractions over a broad range of CO_2 density, from low-pressure gases to the supercritical fluid state. Another goal of these studies is to determine if muonium is long-lived in fluid CO_2 over this broad range of density and thermodynamic conditions. The electronic structure of Mu is basically that of a hydrogen atom, and it can be considered as an ultra-light isotope (mass ~0.11 u) of the-H atom. Whereas H is difficult if not impossible to produce in supercritical fluids, and particularly in $ScCO_2$, let alone to observe its reactions directly on a short time scale, Mu, if formed, can be a probe of H-atom chemical dynamics and interactions in supercritical fluids under a variety of thermodynamic conditions. So far, the only such studies in supercritical fluids have been in supercritical water.[35−37] Since CO_2 molecules do not have the hydrogen-bonding network characteristic of H_2O, it is expected that the comparison of Mu chemistry in $ScCO_2$ with that in supercritical water will lead to valuable new insights on the chemistry of H atoms and free radicals in supercritical fluids.

2. Experimental Procedures

The experiments were performed at the TRIUMF cyclotron facility, in Vancouver, British Columbia. Two target vessels of different design were utilized to cover the pressure range of the experiments, from 10 to 500 bar. Beams of spin-polarized positive muons were momentum selected, collimated, focused onto, and penetrated through metal entrance windows, thereby stopping in the CO_2 sample within either target vessel, which accommodated large variations in density (<0.1 to ~1.1 gcm^{-3}), reflecting the wide range of thermodynamic conditions studied. The vessel used for most of our studies was machined from a cylindrical billet of stainless steel with a 3 mm thick muon entrance window, machined from titanium alloy, and dome-shaped for added structural strength, to accommodate pressures up to 500 bar (Figure 1). Muons of high enough kinetic energy (~25 MeV) were required to pass through this thick window, necessitating the use of backward muons from the M9B channel at TRIUMF, and these studies utilized the SFUMU spectrometer.

Some experiments were carried out at low pressures, in the range of ~10 to 50 bar, but were limited to a small range of temperatures around room temperature. Heating or cooling was accomplished by a controlled flow (a mixture of water/antifreeze) system through a fluid jacket wrapped around the target cell. This cell was also machined from stainless steel, with a muon window of 0.05 mm thickness machined from a solid titanium block, indented to hold a small button muon counter.[38] In this case, lower energy surface muons from the M15 beam line at TRIUMF were used, with the Gas Cart μSR spectrometer, large diameter Helmholtz coils of high homogeneity.

Heating/cooling of the high-pressure cell was accomplished by hot air/liquid nitrogen flow through a fluid jacket. The temperature was monitored by two thermocouples at the two ends of the pressure vessel, as shown in Figure 1, and was controlled by a third thermocouple (position 1) via a PID controller. The thermocouple probes were inserted into small holes drilled into the back and body of the high-pressure sample cell. The maximum temperature gradient at the highest (348 K, Table 1) and lowest temperature (233 K) was ±1 K across the three positions 1, 2, and 3 in Figure 1. It was assumed that the temperature of the fluid inside the pressure vessel is the same as that measured by the thermocouples at its surface. Offline

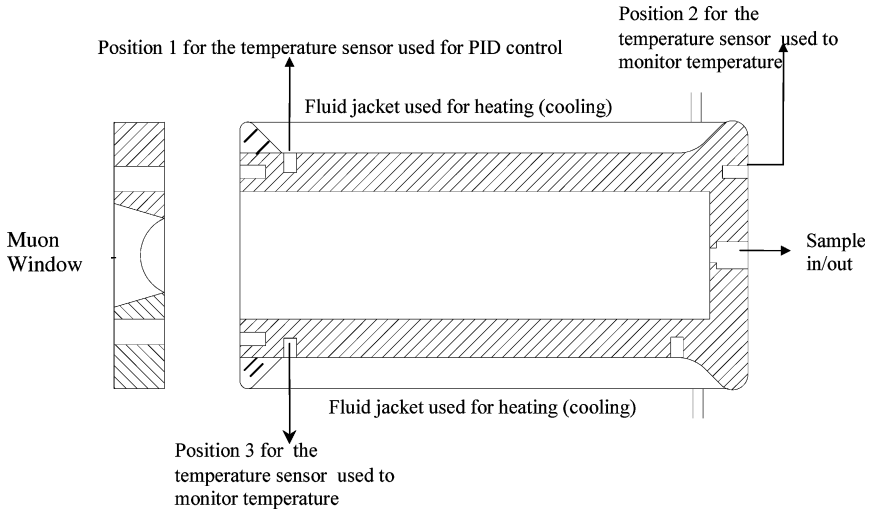

Figure 1. Schematic diagram of the principal components of the high-pressure target vessel showing thermocouple positions and the muon entrance window.

TABLE 1: Muonium (P_{Mu}), Diamagnetic (P_D), and Lost Fraction (P_L) Muon Fractions in Pure CO_2 as a Function of Temperature (T), Pressure (P), and Density (ρ)

T/K	P/bar	ρ/g cm^{-3}	P_{Mu}	P_D	P_L
309	15	0.028	0.84 (9)	0.16 (2)	0.00 (9)
309	46	0.104	0.81 (5)	0.18 (1)	0.01 (5)
329	51	0.104	0.80 (4)	0.18 (1)	0.02 (4)
348	56	0.104	0.81 (3)	0.18 (1)	0.01 (4)
283	39	0.104	0.80 (3)	0.18 (1)	0.02 (4)
309	59	0.152	0.79 (4)	0.19 (2)	0.02 (5)
308	74.8	0.275	0.74 (13)	0.09 (6)	0.17 (15)
309	86	0.612	0.74 (13)	0.13 (3)	0.13 (15)
301	105	0.802	0.68 (12)	0.09 (3)	0.23 (14)
309	215	0.873	0.46 (8)	0.17 (4)	0.37 (11)
309	235	0.888	0.45 (8)	0.16 (3)	0.39 (11)
309	335	0.943	0.42 (7)	0.18 (4)	0.40 (11)
233	42	1.126	0.15 (3)	0.22 (4)	0.63 (7)

tests with the pressure vessel of refs 25 and 36, which was similar to the one used in this work (made from the same material and almost the same geometry), did measure the temperature profile inside the pressure vessel as compared to the temperature at a similar thermocouple position to that of position 2 in Figure 1. In that study, after thermal equilibration and even up to 723 K, the temperature measured ~2 mm from the inner surface of the vessel, filled with water at similar pressures to the present study, was very close to the external thermocouple reading. Since the thermal conductivity of both fluids at comparable reduced temperatures and pressures is similar,[39,40] our assumption of thermal equilibrium between the outer and the inner walls of the pressure vessel is justified. From those studies as well as our recent offline tests of the temperature profile inside the pressure vessel of the present study, filled with 1 atm air, it is estimated that the maximum temperature variation inside the vessel is ±3 K, at the highest and lowest temperatures of Table 1, which has a relatively small effect on density.

Figure 2 shows a block diagram of the setup for sample introduction and pressure/temperature control for the high-pressure target arrangement and the SFUMU magnetic spectrometer. The positions of the muon and positron detectors, plastic scintillators, which give fast timing signals, as well as the SFUMU Helmholtz coils, are also indicated. The pressure vessel of Figure 1 was centered in these coils, oriented so that the magnetic field was transverse to the muon spin polarization. Gas samples (from commercial bottles) were introduced and vented/pumped out through high-pressure stainless (316) steel tubing. Once the sample was added and the temperature and pressure equilibrated, the target vessel was valved off. A cryopumping technique was used to adjust the pressure upward, to 500 bar CO_2, with the indicated cryocylinder (Figure 2) also acting as a ballast volume (~300 mL). If necessary, extra pressure could be vented via high-pressure valves, controlled as well by two relief valves that were set to a pressure of 520 bar. The arrangement in Figure 2 allows independent control of sample temperature and pressure. The pressure was monitored with either of two pressure gauges, one with 0.25 bar accuracy for pressures up to 100 bar and one with 1 bar accuracy for higher pressures. All elements of the high-pressure side of the set up (connecting tubing, relief valve, and valves) were rated to more than 500 bar, as determined by 2/3 engineering-burst constraints of the muon entrance window.

3. Muon Polarization and μSR Measurements

In contrast to conventional magnetic resonance studies, where bulk polarization is a consequence of differing Boltzmann populations in high magnetic fields, in μSR the muon polarization is intrinsic to the probe and is a direct consequence of the nuclear weak interaction. In the decay sequence $\pi^+ \rightarrow \mu^+ \rightarrow e^+$, the muon is produced 100% spin polarized from pion decay, and the (detected) positron is subsequently emitted preferentially along that spin direction, providing a remarkably sensitive measure of the interactions of the muon spin with its environment.[4,20,36,41−45]

Spin polarized positive muon beams are produced at nuclear accelerators such as TRIUMF at MeV kinetic energies (4.1 MeV for surface muons) and enter and stop in the target vessel. Detectors in coincidence define muons entering the sample and positrons emitted when the stopped muons decay. Two pairs of positron detectors were arranged above and below the sample vessel, in the plane of the muon spin precession (Figure 2). In a μSR experiment, the elapsed time between the stop of each muon, registered through a muon coincidence (and starting a time digitizer, TDC) and the detection of its decay positron (stopping the TDC) is measured, and the data are collected and binned in a histogram of counts as a function of time. The probability of detecting the decay positron in a given direction varies as the muon spin precesses in the magnetic field. Thus, μSR histograms obtained from each pair of positron detectors contain oscillations in the muon decay spectrum, and these

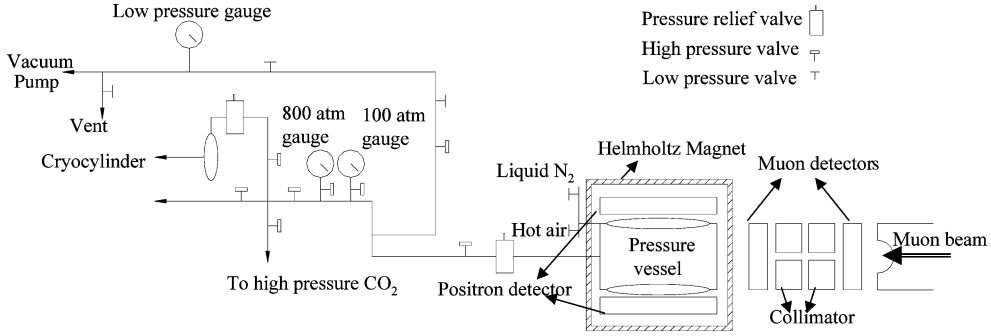

Figure 2. Schematic block diagram of the setup for high-pressure measurements, showing as well the arrangement of the muon and positron counters and the location of the Helmholtz coils on the SFUMU μSR Spectrometer at TRIUMF.

oscillations correspond to the time dependence of the muon polarization.

Each histogram has the form

$$N(t) = N_0 e^{-t/\tau_\mu}[1 + A(t)] + b \quad (1)$$

where N_0 is an overall normalization that depends on a number of factors, such as the solid angle of the positron detectors and the number of stopped muons, b represents random accidental (background) events, $\tau_\mu = 2.197$ μs is the muon lifetime, and $A(t)$ is the asymmetry, which represents the μSR signal of interest and is similar to free induction decay (FID) in magnetic resonance. The asymmetry parameter includes contributions from all muon environments, paramagnetic Mu, and free-radical species as well as diamagnetic species

$$A(t) = \Sigma_i A_i \exp(-\lambda_i t) \cos(w_i t + \varphi_i) \quad (2)$$

where A_i is the initial amplitude of the muon fraction i in a given environment, λ_i is the relaxation rate of the muon spin in that environment, w_i is the corresponding precession frequency, and φ_i is the initial phase for this fraction. The parameters of interest (A_i, λ_i, and w_i,) are extracted from fits of eqs 1 and 2 to experimental data (e.g., Figure 3) and give information, respectively, on Mu formation, kinetics, and hyperfine interactions (in Mu or muoniated radicals), depending on the focus of a given experiment.

An example of Mu precession is shown in Figure 3 (top), in a field of 6 G, for two different CO_2 densities, close to the limits of the density range of the present study. At this field, the Mu atom exhibits a classical triplet Larmor precession, $\upsilon_{Mu} = 1.39$ MHz/G. The solid line shown is a fit of eqs 1 and 2 to the data, for two environments, Mu (the rapid oscillations seen) and diamagnetic. At such a low field, the diamagnetic Larmor precession frequency, $\upsilon_\mu = 13.55$ kHz/G, cannot be seen over the short time range shown in Figure 3 but shows up characteristically over longer time ranges and at fields ~100 G. An example is shown in Figure 3 (bottom), at a field of 90 G, giving a clear slow precession frequency of 1.22 MHz. The middle spectra of Figure 3 show the fast oscillations and slower beat frequency characteristic of two-frequency Mu precession, defined by eqs 3 and 4, and reflecting allowed transitions between muon-electron energy states in a magnetic field,[25]

$$\upsilon_{12} = \frac{1}{2}[(\upsilon_e - \upsilon_\mu) - [(\upsilon_e + \upsilon_\mu)^2 + A_\mu{}^2]^{1/2} + A_\mu] \quad (3)$$

$$\upsilon_{23} = \frac{1}{2}[(\upsilon_e - \upsilon_\mu) + [(\upsilon_e + \upsilon_\mu)^2 + A_\mu{}^2]^{1/2} - A_\mu] \quad (4)$$

Here, υ_e is the electron Larmor frequency and υ_μ the muon Larmor frequency of the coupled two-spin system, with A_μ the corresponding muonium hyperfine frequency. It can be noted in weak fields, <10 G, $\upsilon_e + \upsilon_\mu$ is $\ll A_\mu$, in which case $\upsilon_{12} = \upsilon_{23} = \upsilon_{Mu}$, giving the coherent Mu precession signals seen in Figure 3 (top). The two-frequency precession in Figure 3 (middle) is most easily seen in a Fourier transform spectrum, an example of which is shown in Figure 4, at a field of 110 G. The much slower diamagnetic frequency (~1.5 MHz) is off scale.

The total Mu amplitudes are most easily found in weak fields, <10 G, giving a single amplitude, as demonstrated by the plots in Figure 3 (top), while the diamagnetic amplitudes were found from fields at ~90 G, as in Figure 3 (bottom). The total Mu amplitudes could also be determined from the two-frequency precession signals of the higher field data (Figure 3, middle), but these were always the same, within errors, to A_{Mu} found from the weak field data, which was the method of choice.

Since knowing the absolute muon polarization is important, studies were first carried out in the same pressure vessel with standard samples of N_2 at different pressures, at room temperature, since the absolute polarizations for N_2 have been established previously, over wide density ranges.[33] Comparison of the ratio of measured muonium/diamagnetic amplitudes with these known fractions in N_2 provided a determination both of the diamagnetic signal due to muon stops in the cell window and walls of the pressure vessel, as well as the total muon asymmetry, corresponding to the full polarization at different densities. The measured amplitudes in the CO_2 samples of interest were then corrected according to established procedures:[25,33]

$$P_D = (A_D - A_W)/(A_S - A_W) \quad (5)$$

and

$$P_{Mu} = 2A_{Mu}/(A_S - A_W) \quad (6)$$

where A_D is the diamagnetic amplitude, A_W is the sum of the wall and window amplitude, A_S is the amplitude of the standard (N_2), and A_{Mu} is the muonium amplitude. The factor two in eq 6 accounts for nonobserved singlet muonium.

Supercritical grade CO_2 (99.9995%) was used for these studies, although it was found to be relatively impure since an appreciable relaxation rate of the Mu signal amplitude, λ_{Mu} in eq 2, was observed. This could have been a real effect (e.g., Mu + CO_2 reactions, but repeated studies revealed it was mainly due to reactions with impurities (probably O_2 and CO), which were minimized by alternate freeze/pump/thaw cycles prior to transfer to the pressure vessel, until any remaining dephasing of the Mu signal could largely be attributed to the effects of

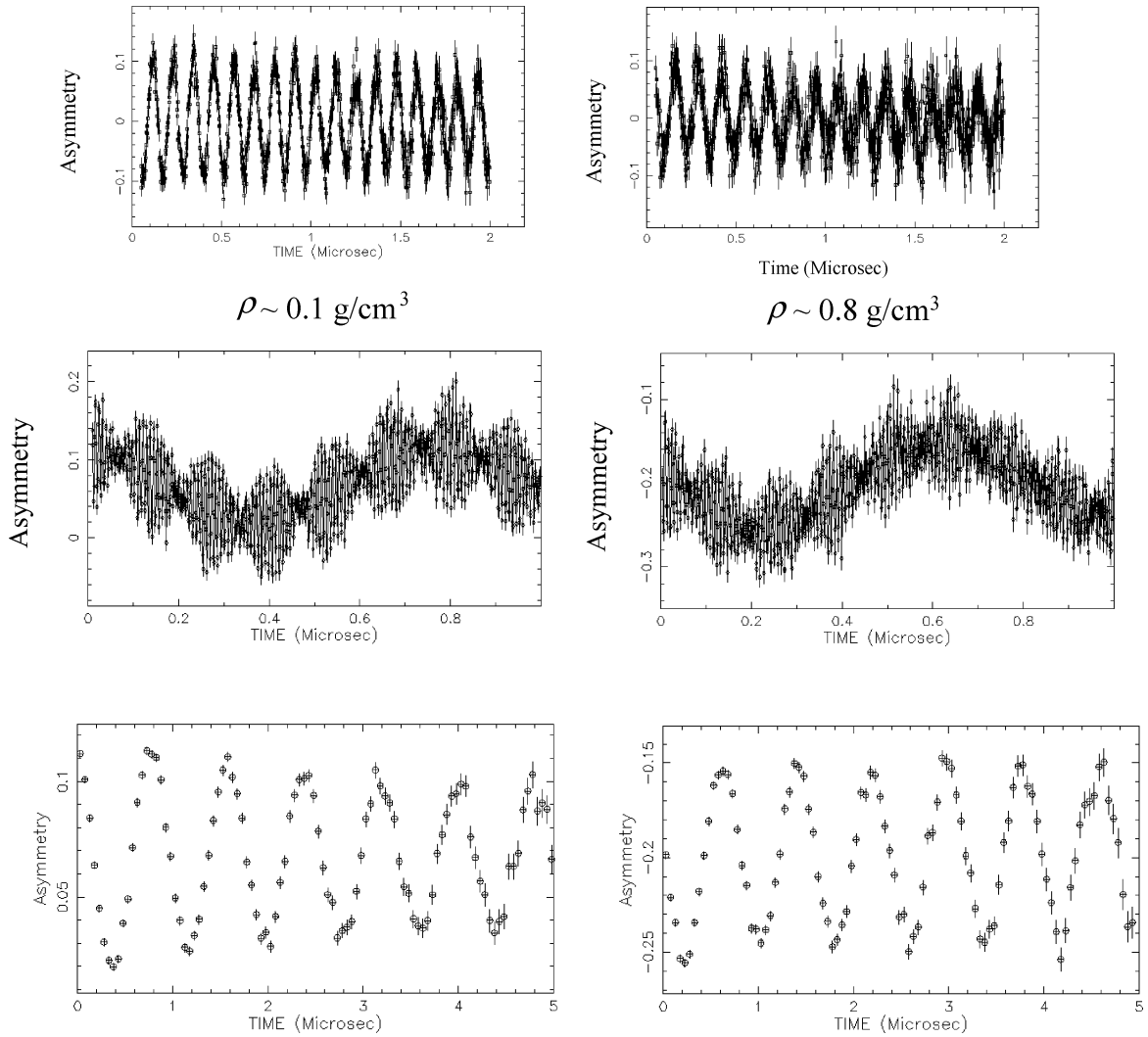

Figure 3. Mu precession in a TF of 6G (top) and 90G (middle and bottom) for two different CO_2 densities. The solid lines are fits of eqs 1 and 2 to the data. In the 6G field, only a single Mu frequency is seen, but this is split into two frequencies at higher fields, giving the beating patterns evident in the middle spectra. There is a slow underlying oscillation due to diamagnetic precession, which is clearly revealed by coarse binning in the bottom spectrum, over a much wider time range.

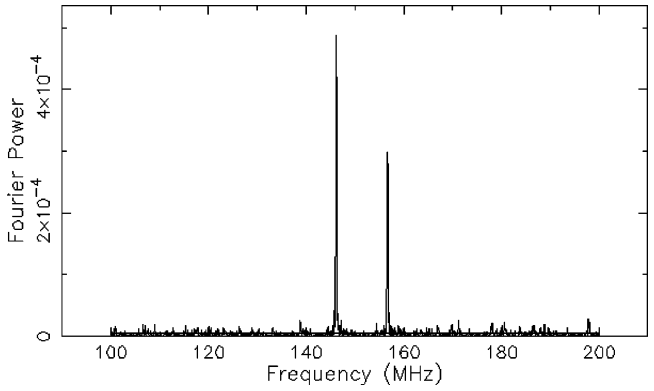

Figure 4. Two-frequency Mu signals, ν_{12} and ν_{23} (eqs 3 and 4) in a TF of 110 G at 100 bar and 34 C in $ScCO_2$. The much slower diamagnetic frequency, at ~1.5 MHz, is off scale.

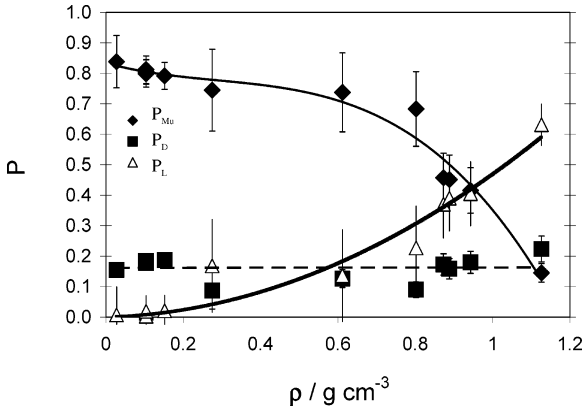

Figure 5. Plots of muon polarization fractions for muonium (P_{Mu}), diamagnetic (P_D), and the missing or lost fraction (P_L), as a function of density in CO_2. The lines are drawn merely to guide the eye.

field inhomogeneity. This was established as well by studies in ultrahigh pure nitrogen (99.9995%), where thermal chemical reaction with N_2 is not possible.

4. Results

The central goal of the present experiments, to determine the fraction of muon polarization in CO_2 over a wide density range, is seen in the results listed in Table 1 and plotted in Figure 5. The CO_2 densities were determined from temperature and pressure readings with the aid of standard reference data.[46] In each case, the polarization fractions for Mu (P_{Mu}) and diamagnetic species (P_D) have been determined from measured initial μSR amplitudes, A_{Mu} and A_D of eqs 1 and 2, as in Figure 3, corrected for wall contributions as in eqs 5 and 6.

TABLE 2: Representative Muonium Relaxation Rates (λ_{Mu}) in Pure N_2 as a Function of Temperature (T), Pressure (P), Density (ρ), Momentum (p), and Magnetic Field (B)

magnet	T/K	P/bar	ρ/g cm^{-3}	p/Me Vc^{-1}	B/G	$\lambda_{Mu}/\mu s^{-1}$	±
gas cart	300.4	5	0.006	30.8	92.6	0.73	0.033
gas cart	300.4	5	0.006	30.8	6	0.34	0.004
gas cart	300.2	58.5	0.066	30.8	6	0.15	0.004
gas cart	300.2	58.8	0.066	30.8	92.6	0.20	0.018
SFUMU	297.1	120	0.135	70	110	0.48	0.015
SFUMU	297.1	165	0.181	70	6	0.43	0.009
SFUMU	297.1	165	0.181	80	6	0.35	0.009
SFUMU	297.1	165	0.181	70	110	0.49	0.011
SFUMU	297.1	165	0.181	70	6	0.33	0.012
SFUMU	297.1	245	0.255	70	110	0.36	0.016
SFUMU	297.1	325	0.316	90	110	1.77	0.089
SFUMU	297.1	325	0.316	70	110	0.40	0.015
SFUMU	297.1	500	0.415	70	110	0.30	0.022

TABLE 3: Representative Muonium Relaxation Rates (λ_{Mu}) in Pure CO_2 as a Function of Temperature, Pressure, Density, Momentum, and Magnetic Field

magnet	T/K	P/bar	ρ/g cm^{-3}	p/Me Vc^{-1}	B/G	$\lambda_{Mu}/\mu s^{-1}$	±
gas cart	309	15	0.028	30.1	6	0.10	0.004
gas cart	309	15	0.028	30.1	135	0.22	0.016
SFUMU	455	73	0.092	75	100	0.95	0.028
SFUMU	455	73	0.092	70	100	0.77	0.041
gas cart	309	48	0.110	30.8	6	0.07	0.003
gas cart	308.7	48	0.110	30.8	98	0.13	0.008
SFUMU	305	54	0.137	75	100	0.57	0.019
SFUMU	305	54	0.137	75	6	0.21	0.008
gas cart	309	58.7	0.151	31	94	0.36	0.023
gas cart	309	58.7	0.151	30	94	0.43	0.018
SFUMU	455	130	0.173	70	100	0.43	0.013
SFUMU	310	75	0.252	70	90	0.23	0.011
SFUMU	308	73.8	0.257	90	6	0.36	0.016
SFUMU	307	76.5	0.322	90	6	0.38	0.02
SFUMU	333	120	0.434	70	90	0.37	0.025
SFUMU	309	86	0.588	90	107	0.46	0.022
SFUMU	306	80	0.614	70	90	0.29	0.017
SFUMU	305	176	0.861	90	110	0.42	0.035
SFUMU	305	275	0.928	90	109	0.55	0.064
SFUMU	310	425	0.975	90	90	0.38	0.025
SFUMU	306	500	1.011	90	6	0.26	0.144

In addition to the values in Table 1, there are several other important results emerging from this work. The first is that muonium could be detected over the whole range of conditions studied, from −40 to 85 °C over a large range of pressures, up to 500 bar, giving densities that ranged from 0.028 g cm^{-3} (26 °C, 15 bar) to 1.2 g cm^{-3} (50 bar and −40 °C). In fact, this is the widest density range ever reported in a μSR experiment. Second, the splitting between the two frequencies at intermediate magnetic fields (Figures 3 and 4) is consistent with a hyperfine coupling constant essentially due to that of vacuum Mu-precession, A_μ ~4463 MHz, albeit slightly reduced (by about 0.2%), due to interaction of Mu with the surrounding CO_2 molecules. Surprisingly, despite significant differences in the intermolecular interactions in water and in CO_2, this value is very similar to what has been reported in supercritical water.[36] That there are no frequencies evident in Figure 4, other than those due to Mu precession, also demonstrates that no MuOCO (or MuO) radical is observed under any thermodynamic conditions and hence that the initial 100% muon polarization is found among only two environments: muonium (P_{Mu}) and diamagnetic (P_D).

Another important point is that the Mu precession signal is long-lived at all densities (Figure 3, top and Tables 2 and 3). Muonium relaxation rates, λ_{Mu}, are reported for different magnetic fields and in different μSR spectrometers over the range of densities studied in N_2 and in CO_2 in Tables 2 and 3, respectively. Thus, in high-purity N_2, λ_{Mu} ranges from 0.1 to 1.8 $^{-1}\mu$s as the thermodynamic conditions, magnetic field, and momentum is varied, partly reflecting the effects of field inhomogeneity arising from differing muon stopping distributions (Table 2); it is generally larger at higher magnetic fields, is sensitive to the selected momentum, and is typically smaller in the more homogeneous field of the gas cart spectrometer than in the SFUMU magnet. The CO_2 data in Table 3 are similar. The scatter in these values is likely due to additional effects of trace impurities in both the N_2 and CO_2. However, even at the highest densities, where chemical reactions of Mu would be most important, λ_{Mu} shows no significant increase from that found at lower densities, demonstrating that Mu is unreactive with CO_2, on a μs scale.

5. Discussion

5.1. Muonium Formation and the Hot and Spur Models.

The results of the current experiments, on the distribution of muon polarization in CO_2, reflect the mechanism(s) at play in μ^+ thermalization processes in matter. To put these mechanisms in perspective, some preliminary remarks on the general aspects of ion thermalization as well as on the two mainly opposing models that have characterized debate in the field of μ^+ thermalization processes for the past 25 years[18−26,28−33] will be presented here.

The initial stage of the energy loss process of any ion in matter is Bethe−Bloch ionization.[16,17,47] After passing through the entrance window of the target cell (Figures 1 and 2), muons entering the sample still have the MeV kinetic energies noted earlier, many orders of magnitude higher than those of chemical interest. Most of this initial energy is dissipated in ionization and excitation processes, described by the Bethe−Bloch stopping-power formula for $-dE/dX$. During this regime, there is no loss of muon polarization.

In a low-density gas, this is followed by a regime of cyclic charge exchange with moderator M beginning around 100 keV for the positive muon and described by

$$\mu^+ + M \xrightarrow{\sigma 10} Mu + M^+$$
$$Mu + M \xrightarrow{\sigma 01} \mu^+ + M + e^- \qquad (7)$$

with average electron capture (σ_{10}) and loss (σ_{01}) cross-sections, together with those for elastic and inelastic energy moderation, determining the outcome.[33,41,48−51] In this regime, lasting down to an energy E_{min} ~10 eV, the muon undergoes about 100 cycles in a time <1 ns (at 1 atm in the gas phase),[41,50] emerging as either a bare μ^+ or as the Mu-atom, prior to entering its third thermalization stage, from E_{min} to k_BT. In this final stage of energy loss, Mu may undergo hot atom reactions and as well the μ^+ may continue to form Mu by charge exchange and/or to form muon molecular ions, MMu^+ both in competition with elastic and inelastic scattering.

In dense media like liquids or in the supercritical state, the binary collision assumption of charge exchange and energy moderation is not valid, as shown by studies of the radiation chemistry of ionizing beams in liquid phase.[52−54] In supercritical fluids, the situation is even more complex due to the sensitivity of secondary radiolysis reactions on cage effects, diffusion, and solvation that depend on the density of the fluid.[4,5,11−15,36−37]

The degree to which charge exchange, energy moderation, and hot atom reactions influence the distribution of muons between diamagnetic and Mu fractions under such conditions is not known, but from the works of refs 33 (in N_2 and C_2H_6) and 25 (in supercritical water), it appears that these processes alone cannot explain the density dependence seen above $\sim$0.01 g/cm^3, meaning that other processes must be competing.

The three stages for energy loss processes in the gas phase are usually replaced with the (1) physical stage, (2) physicochemical stage, and (3) chemical stage in condensed media,[16,55−56] which also overlap to some extent. The physical stage includes Beth−Bloch ionization, charge exchange, the production of secondary electrons with energies $\gtrsim$100 eV, and energy loss to electronic states. All of these processes are believed to occur in $\lesssim$0.1 fs. The physicochemical stage includes fast ion−molecule reactions and proton-transfer reactions, which occur in $\lesssim$10 fs. It also includes electron solvation, self-diffusion times, and spur formation on a time scale of $\lesssim$ps. The chemical stage includes further spur and intra track reactions happening on a $\lesssim\mu$s time scale and further chemical reactions that would not be relevant to the process of Mu formation, due to their long time scales.

Accordingly, there are two schools of thought on the mechanism of Mu formation in condensed media, the spur and hot atom models.[18−26,28−30] Common to both models is the assumption that the μ^+ causes ionization and undergoes charge exchange in its initial thermalization processes (physical stage): what differs between them is the view at the end of this period, in the final thermalization regime from E_{min} $\sim$10 eV to k_BT.

The essence of the hot atom model, well-supported in the low-density gas phase, is that Mu* reactions deplete the Muonium amplitude (P_{Mu}) and increase the diamagnetic yield (P_D) in reactive encounters at epithermal (few eV) energies.[51,57,58] These kinds of reactions are typically direct (H-atom) abstraction reactions, as in alkane (RH) gases forming MuH, or substitution reactions, forming MuR*, giving rise to pressure-dependent yields in the gas phase.[33,51,59] Hot atom addition reactions in unsaturated gases, forming muoniated free radicals (P_R), may also occur,[60] MuOCO* being of interest here. In the case of inert gases, where hot atom reactions are unlikely or impossible (e.g., noble gases), the diamagnetic environment has been shown to be due solely to the formation of muon molecular ions (e.g., $NeMu^+$), estimated to form at energies near $\sim$1 eV[61,62] in the final stage of thermalization. These latter studies have also demonstrated that there are no free (bare) μ^+ in gases at observation times, and by implication, not in the liquid-phase either. Such hot ion reactions, occurring within the physicochemical stage, also give rise to molecular ion environments in condensed media, and they are intermediates in the spur model (e.g., $RHMu^+$ in eqs 9 and 10).

The central tenant of the spur (radiolysis) model is that an epithermal muon or molecular ion ($MuCO_2^+$ in the present study) is postulated to thermalize close to the end of its track, and the observed distribution of muon polarization is determined by the outcome of competitive reactions between muoniated and spur transients, as in eqs 8−16. Reactions in the terminal spur, contributing to P_D, P_{Mu}, and P_L, have been postulated to occur in a variety of media but mainly investigated to date in saturated hydrocarbons and H-bonded solvents such as H_2O and alcohols, collectively denoted here RH, (see ref 31 and references therein for work in condensed noble gases) and described by the following kinds of reactions[18−26,33]:

$$\mu^+* + e^- \rightarrow Mu* \quad (8)$$

$$\mu^+* + RH \rightarrow RHMu^+* \quad (9)$$

$$RHMu^+* + RH \rightarrow RHMu^+ + RH \quad (10)$$

$$RHMu^+ + e \rightarrow Mu + RH \quad (11)$$

$$RHMu^+ + RH \rightarrow RMu + RH_2^+ \quad (12)$$

$$Mu + e_{sol}^- \rightarrow \text{spin depolarized Mu} \quad (13)$$

$$Mu + R \rightarrow \text{spin depolarized Mu} \quad (14)$$

$$Mu + e_{sol}^- \rightarrow MuH + R^- \quad (15)$$

$$Mu + R \rightarrow RMu \quad (16)$$

where R is any paramagnetic transient arising from RH, except the solvated electron. It is noted that the μSR technique, with a frequency resolution given by $1/\tau_\mu$ 0.5 MHz, cannot distinguish bare μ^+ from diamagnetic molecules such as MuH or molecular ions such as $RHMu^+$, so all contribute to the diamagnetic fraction, P_D. Also the electron in eq 11 can be both solvated and pre-solvated; the latter is essentially a free electron.

As indicated, both reactions 8 and 11 can produce Mu.[18−26] Solid evidence for this has been obtained from electric-field experiments in some liquefied inert gases.[31,63,64] These studies proposed a delayed mechanism for Mu formation based on evidence that bare muons or muon molecular ions (indistinguishable) and electrons come together from some distance by their coulomb interaction to form Mu (eqs 8 and 11), no matter what the time scale is. This point seems to be often misunderstood, as in the recent fast scavenging studies in several (saturated) liquids reported in refs 29 and 30, where the authors remark that Mu forms in much shorter times than the delayed μs time scale proposed in the calculations of Siebbeles et al.[32]

A further important result of the electric-field experiments of refs 31, 63, and 64 is germane to the present study: the time scale of delayed muonium formation depends on the electron mobility as well as on a given muon−electron distance and can be anywhere from several μs, for extended distances on the order of 500 Å or very slow electron mobility,[31,63,64] to sub-ps, if the muon happens to thermalize very close to the track electron or if the mobility of the electron is very high. These electric field studies have conclusively shown that even early time muon−electron track interactions can be interrupted, giving a decreased yield for P_{Mu} or increased P_D. Much longer times, consistent with the μs time scale commented on in refs 29 and 30, contribute very little to P_{Mu} in TF-μSR, due to Mu dephasing effects, and contribute instead to the lost fraction, P_L, a point nicely illustrated in the calculations of ref 32.

Although the studies of ref 29 and 30 are consistent with earlier works[18−19,22−25] in suggesting that P_{Mu} and P_D in liquids form on a fast time scale, comparable to the ps slowing-down time expected in liquids, they depart considerably from these earlier studies in concluding that hot Mu* (or hot muon) reactions dominate, to the exclusion of any radiolysis effects in determining the Mu, P_{Mu}, and diamagnetic yields, P_D, based on their conclusion that P_D is formed in $\lesssim 10^{-10}$ s. As already commented and consistent as well with the aforementioned electric field studies, within the radiolysis model, Mu and

diamagnetic muon fractions could be formed in less than a ps. The conclusion of refs 29 and 30 is also at variance with measured P_D values in gaseous hydrocarbons over wide pressure (density) ranges, which concluded that hot Mu-atom reactions alone could not account for these yields.[33,59]

Of the radiolysis steps shown previously, eqs 9, 10, and 12 along with hot Mu* reactions contribute to P_D on a similar fast ($\lesssim$ps) time scale as for Mu formation. Eqs 13−15 in the spur contribute to the lost fraction, P_L, by electron spin exchange with paramagnetic species, as do eqs 15 and 16, leading to unobservable diamagnetic final products in TF environments, on the much slower time scale of the expanding track, ∼1−100ns.[18−25]

5.2. Comparison of Results in $ScCO_2$ with Those for C_2H_6 and ScH_2O. Despite the very different molecular structure and properties of H_2O and CO_2, it is noteworthy that in both of these environments, Mu is unreactive at thermal energies over a similar range of densities (Table 3 and refs 25, 35, and 37). As in ScH_2O,[25,36] muonium was unambiguously identified by its measured hyperfine- coupling constant (Hfc), ∼4463 MHz, determined from the υ_{12} and υ_{23} frequencies of eqs 3 and 4 at fields ∼100 G (Figure 4). It was important to establish this since in weak transverse fields (e.g., Figure 3, top), with no nuclear moments other than the muon itself (ignoring the ∼1% ^{13}C), Mu and either of the MuOCO or MuO radicals would have the same precession frequency. Our current calculations also show that the formation of these muoniated radicals would have led to order-of-magnitude smaller hyperfine coupling constants.[65] This is the first report of its kind in $ScCO_2$, which compliments previous work in ScH_2O,[25,36] the only reports to date on any H-atom isotope in supercritical fluids.

One of the principal findings of this work, bearing on the subject of radiation chemistry, is that there was little variation in the fractions of muon polarization with density in CO_2, until high densities, $\gtrsim$0.8 g/cm^3, well above the critical density of $\rho_c = 0.468$ g/cm^3, as shown by the data in Table 1, plotted in Figure 5. Note, from the entries in Table 1, that it is change in density not temperature or pressure that is important here. To put the density trends in Figure 5 in perspective, the polarizations P_D, P_{Mu}, and P_L in CO_2 are compared with similar μSR data sets from recent studies in supercritical water,[25] over comparable ranges of density, and with earlier data in C_2H_6[33] in Figures 6−8, respectively. While the ScH_2O and C_2H_6 data show similar trends with density, there are significant differences in the case of $ScCO_2$, which clearly reflect different mechanisms for the distribution of muon polarization in these fluids.

Though not discernible from the plots of Figures 6−8, at very low densities, in both C_2H_6[33] and water vapor,[51] there is an increase in both P_D and P_{Mu}, and in parallel a decrease in P_L to zero, such that $P_D + P_{Mu} \rightarrow 1.0$. This effect is due to the quenching of depolarization in the cyclic charge exchange regime, when the time between bimolecular collisions becomes much less than the inverse of the muon-electron Hfc, ∼0.2ns, corresponding to CO_2 densities $\gtrsim$0.01 g/ cm^{-3}. With increasing density, for both H_2O and C_2H_6, increases in P_D (Figure 6) are mirrored primarily by decreases in P_{Mu} (Figure 7), with relatively little change in P_L (Figure 8) at the highest densities relevant to the current study. In contrast, for CO_2, P_D remains essentially constant over the whole density range, with the decrease in P_{Mu} seen at the highest densities mirrored instead in an increase in the lost fraction, P_L.

Interestingly, for CO_2, P_L stays close to zero over a much wider density range, up to $\gtrsim$0.1 g cm^{-3} (Figure 8) but then begins to increase noticeably at the higher densities, where most of the data has been obtained, reflecting the importance of other depolarization mechanisms at these densities.

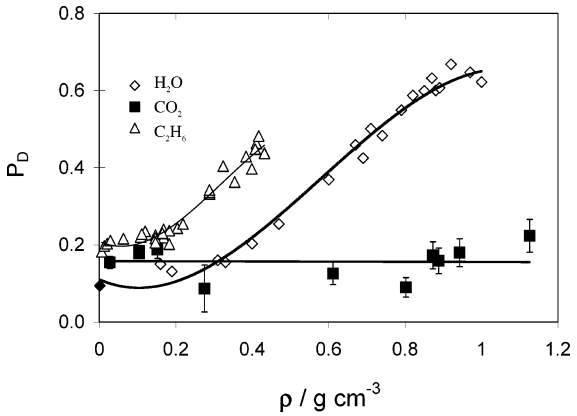

Figure 6. Diamagnetic (P_D) fractions in pure CO_2, H_2O, and C_2H_6 as a function of density (for clarity, the error bars for C_2H_6 and H_2O data are not shown). Data for H_2O and C_2H_6 taken from refs 25 and 33, respectively. The lowest density data point for water, represented by the black diamond, is from ref 51. The lines are again drawn to guide the eye.

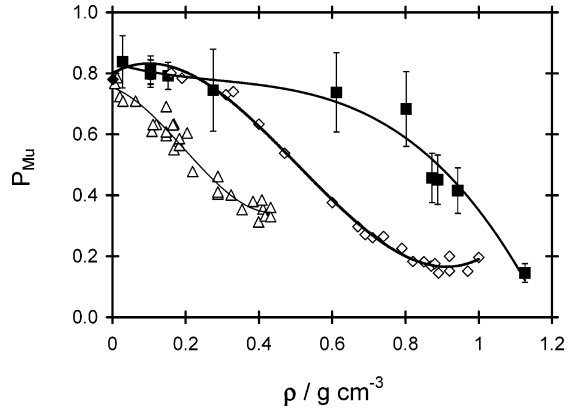

Figure 7. Muonium (P_{Mu}) fractions in pure CO_2, H_2O, and C_2H_6 as a function of density. See caption to Figure 6.

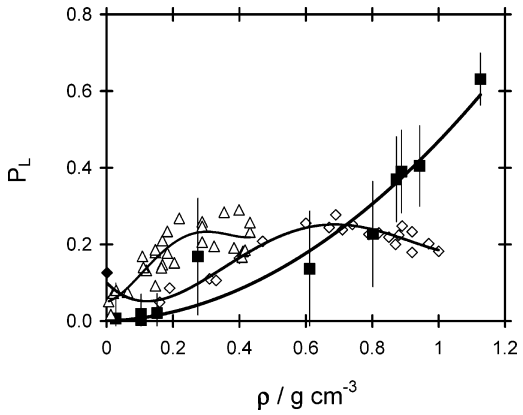

Figure 8. Lost fractions (P_L) in pure CO_2, H_2O, and C_2H_6 as a function of density. See caption to Figure 6.

In the hot atom model, Mu* abstraction and substitution reactions in C_2H_6 and H_2O can be expected to cause an increase in P_D at the expense of P_{Mu}. Previous studies on C_2H_6 and in other alkanes as well have shown that hot atom reactions cause logarithmic increases in P_D with (gas-phase) density up to an asymptotic limit, corresponding to $P_D \sim 0.25$ for C_2H_6, only half of the highest density values plotted in Figure 6. While substitution reactions do give density dependent Mu* yields, the asymptotic nature of these yields demonstrates that enhanced

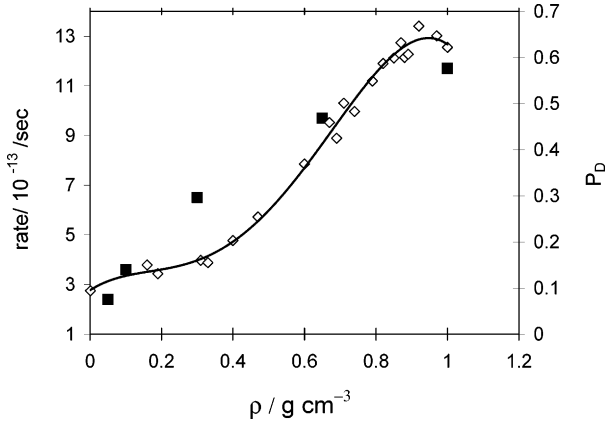

Figure 9. Diamagnetic (P_D) fraction in ScH_2O from μSR studies of ref 25 (diamonds) and rate of proton transfer in ScH_2O (squares) from ref 69 as a function of density. The trend line through experimental data is to guide the eye.

hot atom reactivity alone cannot be responsible for the continued increase in P_D with density seen in Figure 6. It should be noted that the alkane studies of refs 33 and 59 give only an upper limit of the contribution of hot atom reactions since competition with radiolysis (spur) reactions was ignored. Still, the analyses therein as well as more general comparisons of diamagnetic yields in molecular gases at low pressure,[51,57,59] where P_D is ~0.2, with corresponding values for a range of saturated liquids where P_D is typically 0.6,[18−20] strongly suggests that at least half of the observed diamagnetic yield in RH-type liquids is from sources other than Mu* reactivity, including the ion−molecule and proton-transfer reactions indicated in the spur reactions of eqs 10−12.

Several studies in water in particular have in fact demonstrated that radiolytic processes (eqs 8−16) play the main role in determining these yields.[18,19,23−25] Recent results also suggest that there is a strong correlation between the density dependence of P_D and P_{Mu}[25] with the density dependence of the rate of proton transfer in ScH_2O,[66] as shown in Figure 9. Increases of this nature in the rate of proton-transfer reactions with density implied by reaction 12 in H-containing solvents[66−69] cause an increase in P_D with density in μSR experiments since such proton-transfer reactions trap muons in the diamagnetic environment, RMu. Note that over a similar range of density in Figure 9, both P_D and rate of proton transfer increase by the same factor of ~6. Such correlations confirm that radiolytic processes (eqs 8−16) play significant roles in determining P_D and P_{Mu}, the latter decreasing as reaction 11 becomes less competitive.

There are two principal differences between CO_2 and most other fluids that dramatically affect the μSR polarization fractions, seen in the comparisons in Figures 6−8. First, since CO_2 is a hydrogen-free solvent, proton-transfer reactions (eq 12), which play an important role in most previous studies of radiolysis effects, (Figure 9), are completely absent in CO_2. Second, due to its strong C═O double bonds, thermal abstraction reactions are very unlikely since the H-atom reaction (forming OH) is highly endoergic, while the addition reaction forming HOCO has a large activation barrier.[70,71] These effects mitigate even more against the analogue Mu reactions, due to zero-point energy shifts,[72] thus explaining the fact that Mu is long-lived in $ScCO_2$ and the lack of any significant density dependence in the relaxation rate, λ_{Mu} (Table 3).

On the other hand, since, as discussed earlier, hot atom reactions of Mu* with C_2H_6 and H_2O contribute to P_D in competition with radiolysis effects, we could similarly expect Mu* reactions with CO_2 to occur, either abstraction (forming MuO) or addition (forming MuOCO). Both products are free radicals, so would contribute to P_R in this case, but as previously noted there is no evidence for any such radical component (Figure 4). Since the corresponding reactions of H* + CO_2, at ~2 eV, from photolysis in matrixes,[73,74] and in the gas phase,[75,76] are known, why are the Mu isotopomers not observed?

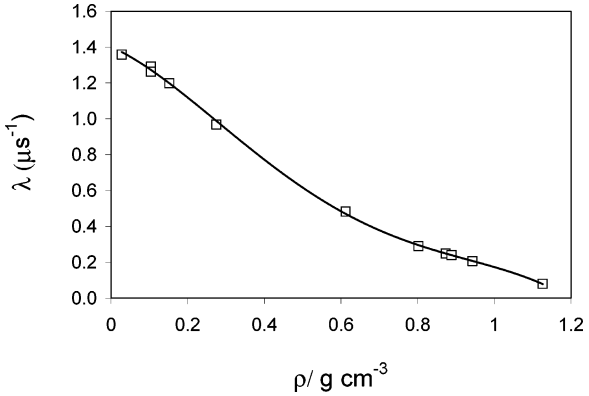

Figure 10. 10. Estimated spin rotation relaxation rates for, λ, MuOCO in $ScCO_2$ at densities corresponding to the thermodynamic conditions of our experiments.

There could be several possible reasons, as follows. In the case of hot-atom abstraction, the MuO radical may be expected to undergo rapid spin relaxation rendering it unobservable; however, since both SeMu and SMu radicals, close relatives of Omu, have been observed in condensed phases[77] and the OH and OD radicals have been observed directly by ESR in the gas phases and in matrixes,[78−80] it seems reasonable to expect that MuO could also be seen here.

Possible as well is hot-atom addition, forming MuOCO*, since epithermal addition is known to occur in Mu* + $C_2H_4 \rightarrow MuCH_2CH_2$, contributing to P_R, even at nominal pressures of a few bars.[60] However, MuOCO* has about half the degrees of (vibrational) freedom and correspondingly a much shorter lifetime than $MuCH_2CH_2$*. On the other hand, it is known that the HOCO radical exists in matrixes[81,82] and more importantly in ~800 Torr of N_2 at room temperature.[83] Furthermore, the HOCO and DOCO radicals are found to be stable in the gas phase at room temperature (τ > 10 ms) at a few Torr pressure,[84] with only a small isotope effect. According to the lifetime calculations for unimolecular decay of HCO2*,[71] following epithermal (~2 eV) H* addition and comparison of dissociation rates for MuO_2* and HO_2*[85], we expect the Mu isotopomer to have a short lifetime, but in any case it would be reasonable to expect MuOCO* to be stabilized by collisions at the high densities (up to 1.0 g/cm^3) of the present studies. On the contrary, the MuOCO radical has not been observed at any density.

Since the formation of OMu and MuOCO by hot Mu reactions is at least a reasonable expectation, the fact that neither is observed could then suggest spin relaxation, due to the intramolecular electron spin-rotation interaction,[6,86−89] causes rapid muon depolarization and hence renders the radical unobservable. If so, this could have led to an increase in P_L at higher densities, from $P_R \rightarrow P_L$, consistent with the data in Figure 8. The spin relaxation rate of MuOCO can be estimated from well-established models in high-density fluids (see, e.g., refs 6, 86−88) with a Δg_e value of 0.002 corresponding to HOCO[90] and viscosities of $ScCO_2$ from ref 91. These are plotted versus density in Figure 10 and as can be seen are very low and most importantly have exactly the opposite trend to the density dependence of P_L in $ScCO_2$ (Figures 5 and 8). We may

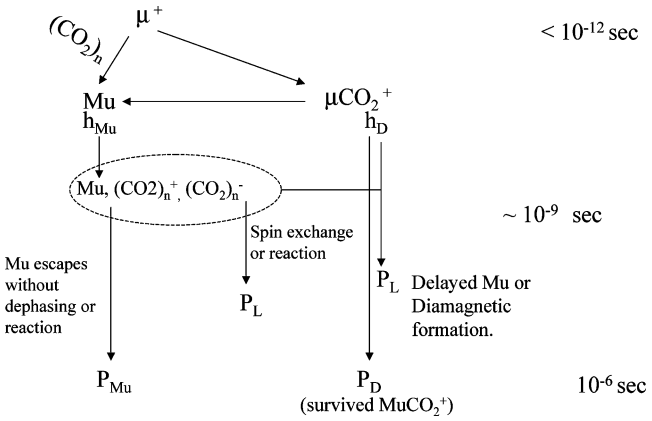

Figure 11. Schematic diagram of the end-of-track radiation−chemical changes induced by implanted muons in $ScCO_2$ at high densities. The fractions labeled "h" signify "hot" and give rise to the observed polarization fractions P_D and P_{Mu}, with $P_L = 1 - (P_D + P_{Mu})$. There is no observed free radical component (P_R) in $ScCO_2$.

expect faster rates for MuO, due to its larger *g*-factor anisotropy, Δg_e, but still with the same density dependence as in Figure 10. These results present convincing evidence that, if formed, MuOCO (or MuO) should have been observed in our experiments.

The remaining possibility accounting for their nonobservation is that little epithermal Mu is formed in dense CO_2 in the first place, and if so, Mu* reactions would be rendered largely inconsequential. In that case, P_{Mu} would be mainly due to charge neutralization reactions of ionic muon environments in the terminal spur, the equivalents of spur eqs 8 and 11, which would otherwise contribute to delayed Mu formation.

Since proton-transfer reactions (eqs 10 and 12) are not possible in CO_2 and since hot atom Mu* reactivity is unlikely and any way could not contribute to the diamagnetic yield, the only source of this yield in CO_2 is formation of the solvated $Mu(CO_2)^+$ ion, formed by epithermal muon capture in accord with eq 9, and with previous gas-phase studies of muon molecular ions.[61,62] This expectation is also in accord with electron-radiation studies in CO2[11−15] as well with previous studies of radiolysis effects in ScH_2O[25] and is reflected in the modified spur model for CO_2 (Figure 11) discussed next.

In contrast to the prompt formation times of the fractions P_D and P_{Mu}, the missing fraction P_L, in high density environments, is believed to be solely due to radiolysis effects on a tens of ns time scale.[18−25] As outlined earlier, intra-spur reactions of muonium lead to this lost fraction (eqs 13−16), and the complex inter-dependence of the competition among these reactions leads to the variation of this lost fraction with density (Figure 8). In marked contrast though to these density-dependences in both C_2H_6 and H_2O, where P_L rises quickly to largely constant values of ~0.2, albeit at somewhat different densities (~0.1 g/cm^3 in C_2H_6 and ~0.5 g/cm^3 in H_2O), that for CO_2 continues to increase (Figure 8).

The lost fraction, due either to electron spin exchange (eqs 13 and 14) in the terminal spur and/or to chemical reactions with the radiolytic-produced species (eqs 15 and 16), with a concomitant decrease in P_{Mu},[19,24] the implication from the present data being that $P_{Mu} \rightarrow 0$ at densities ~1.2 g/cm^3 (Figure 7). Electron spin exchange in an unpolarized environment converts the triplet Mu state $|\alpha_\mu\alpha_e>$, which characterizes Mu precession in weak transvere fields (Figure 3, top), to $|\alpha_\mu\beta_e>$, which is not an eigenstate of the Hamiltonian. Thus, $|\alpha_\mu\beta_e>$ oscillates with $|\beta_\mu\alpha_e>$ on a time scale given by the inverse of the Hfc, $1/A_\mu$ ~0.2ns, thereby flipping the muon spin and hence depolarizing it.[37,41,92,93] Intra-track chemical reactions of Mu forming either muoniated radicals (here MuO or MuOCO) or diamagnetic molecules on a slow time scale lead to dephasing of the spin polarization in a TF, as does delayed Mu formation[31,63,64] (eq 11) and also contribute to P_L. Any fast spin relaxation of muoniated radicals could in principle also contribute to the lost fraction although previous arguments render this unlikely.

The comparisons in Figure 8 refect a number of subtle effects. In the course of the physicochemical stage, the excess negative charge from radiolysis processes becomes a solvated electron, e_s^- trapped in a spherical cavity formed by several solvent molecules. However, the encounter rate between Mu and e_s^- (eq 13) as well as with other paramagnetic transients (R) clearly depends on the transport and relative escape rate of these transients from the spurs, which depends in turn on the diffusion constant of a given transient. The viscosity at a typical low-density condition of Figure 8 in water (e.g., at 200 bar and 375 ×bcC (0.13 g/mL) is 25.9 μPa s,[39] while at the same density in ethane (e.g., 46.5 bar and 30 ×bcC), it is 15.7 μPa s.[94] Assuming a Stokes−Einstein model for the diffusion of Mu as a crude approximation,[37] the diffusion in water is thus ~1.5 times faster than in ethane at these conditions, in accord with the slower increase in P_L with density seen in the data in Figure 8. Another factor is the diffusion of the electrons to the solvent cage where Mu is in the final spur within its track. The electron mobility is much larger in hydrocarbons than in water.[26,95,96] Thus, intra-track spin exchange with electrons can be expected to exhibit a different density dependence in water and ethane, in accord with the different threshold behavior for P_L seen in Figure 8 at lower densities. On the other hand, the concentration and type of radiolytic species are different in these two systems. Even when these species encounter, the efficiency of the spin depolarization and radical recombination reactions will be altered by changes in solvent structure, in particular if the cage effect is no longer effective.[4,5,11−15,36−37] This complexity is seen as well in the case of solvated electrons in $ScCO_2$ (Figure 11) and calls for extensive theoretical computation to draw quantitative conclusions from all the experimental data available.

5.3. Modified Spur Model for Muons in CO_2. To put the present experimental results in CO_2 in perspective in terms of the relevant spur reactions to those given previously, we show in Figure 11 a scheme of radiation processes likely contributing during the final stages of the energy loss processes of muons in high-density $ScCO_2$. This scheme is also based on pulse radiolysis studies of $ScCO_2$,[11−15] which suggests the formation of multimer radical anions and cations $(CO_2)^-_n$, $(CO_2)_n^+$ (mainly $C_2O_4^+$) produced in electron-irradiated $ScCO_2$. These same studies suggest that the attachment rate of electrons to CO_2, forming the equivalent of solvated electrons, increases while the detachment rate decreases, with increasing density, with a $(CO_2)^-_n$ lifetime between 20 and 100 ns in the high-density region. It is believed as well that in this high-density region, each $(CO_2)^-_n$ ion extends to about 1 nm. This picture of an extended size for the solvated electron and the stability of radical anions at higher densities in $ScCO_2$, as well as the fast mobility of any free electrons under the same conditions,[13] is consistent with the interplay seen between P_{Mu} and P_L in the present data, on a similar (~100 ns) time scale of the μSR experiment. It is also similar to the results of the E-field studies in liquid Ne [31] where two type of radiolysis electrons with significantly different mobilities were shown to exist. Theradiolysis processes ocurring on just such tens of ns time scales depend significantly on

density and hence on thermodynamic conditions and that leads to the tunability of radiation chemistry effects in $ScCO_2$.

With reference to Figure 11, and to our earlier discussions, the μ^+ emerges from the physical stage at epithermal energies, either as the Mu atom or remaining as a bare muon. In its further thermalization, the μ^+ can continue to form Mu, but further electron loss from Mu is unlikely, giving rise to the total prompt fraction, h_{Mu}. At lower energies, estimated to be ~1 eV from gas-phase data,[61,62] those μ^+ that have not formed Mu form the muon molecular ion $MuCO_2^+$, or its multimers, by ion-capture reactions in the physicochemical stage, giving the hot diamagnetic fraction, h_D. As previously noted, the initial distribution of muons into the fractions h_{Mu} and h_D occurs on a time scale of $\lesssim 10^{-12}$ s,[18−26] during both physical and physicochemical stages. Once formed, some fraction of the initial amount of muonium, h_{Mu}, which has retained (half of) its initial polarization, undergos electron spin exchange and reactions with the radiolysis products indicated in Figure 11 (both are paramagnetic), giving a contribution to the lost fraction, P_L; and a further fraction escapes, contributing to the observed Mu polarization fraction, P_{Mu}, on a μs time scale. From the inital ionic component contributing to h_D, some fraction may undergo electron capture with solvated electrons, in the form of $(CO_2)^-_n$, forming delayed muonium in time scale of ~10 ns or possibly further dephased diamagnetic environments, both contributing to P_L. However, the fact that the decrease in P_{Mu} seen is paralleled almost exactly by a corresponding increase in P_L (Figure 5 and Table 1) means that P_L in CO_2 is largely due to depolarized Mu, in agreement with long-standing interpretations from muon radiolysis studies.[18−19,22−25,33]

Within the context of processes involved in forming P_D and P_{Mu}, the radiolysis scheme of Figure 11 is also consistent with the aforementioned studies of the effects of E—fields on a range of condensed rare gases[31,63,64] in both the liquid and solid phases, which conclude that the muon-self-track-electron interaction changes from isolated pair (muon plus the nearest track electron) in helium to multipair (muon in the vicinity of tens of track electrons and positive ions) in argon. This would suggest that the equivalents of reactions 8 and 11 contained in the scheme of Figure 11 are between muons and tens of track electrons and solvated electrons in the presence of many multimer cations, in the case of CO_2. Also akin to radiolysis effects in condensed noble gases, the present studies in CO_2 seem to reveal little or no hot Mu reaction, which would have been manifest in a radical fraction, P_R.

With regard to the similarity of the density dependence of the fractions P_{Mu} and P_D in H_2O and C_2H_6 and their differences with CO_2 (Figures 6 and 7), it is again noted that both hot Mu* reactions and/or rapid proton-transfer reactions or hopping mechanisms (Figure 9) that lead to trapping of the muon in a diamagnetic environment (eq 15) and hence contributing to P_D are not possible in $ScCO_2$, explaining both its reduced diamagnetic yield (P_D ~0.2), postulated to be solely due to the ionic environments shown ($MuCO_2^+$, and $Mu(CO_2)_n^+$), and the lack of any density dependence (Figure 6). This is the only μSR study where such a clear contribution to the diamagnetic yield can be identified, over the largest density range that has ever been investigated. The μ^+ reaction scheme of Figure 11 for $ScCO_2$, a rare example of radiolysis or spur effects in a fluid that lacks any proton environment, contrasts in particular with the strong H-bonding effects present in the water. One may expect similar behavior for heavier alpha-particles arising from radioactive decay in waste management and nuclear reactor cycles in $ScCO_2$,[7−9] although in these cases there could also be a complication from partial charge exchange, giving rise to a higher level of multiplicity of ionic envrionments.

6. Conclusions

We have demonstrated the capability to study muonium chemistry in sub- and supercritical CO_2 for the first time. Mu was found to be long-lived on a time scale of a few microseconds, and over a wide density range, from well below to well above the CO_2 critical density, $\rho_c = 0.47$ g/cm^3. Consequently, Mu formation can be used as a uniquely sensitive probe to study radiolysis effects in $ScCO_2$ under the same thermodynamic conditions that exist in radiation-induced polymerization and nuclear waste extraction processes. The contrasting differences in the trend of the density dependence of the diamagnetic fractions in CO_2 (where P_D is constant) as compared to H_2O and C_2H_6 (where P_D increases at the expense of the Mu fraction), strongly suggests that in H-containing solvents the competition of proton (muon) transfer reactions with molecular ion- electron charge neutralization reactions is a key factor in the process of Mu formation and confirms that radiolysis reactions play a significant role in the process of Mu formation in high-density fluids. Being a hydrogen-free solvent, intra-spur proton-transfer reactions that can influence or even determine the observed muon polarization fractions in most other solvents are absent in CO_2. The constant and much smaller diamagnetic fraction is attributed solely to the formation of solvated $MuCO_2^+$ molecular ions, with the lost fraction, P_L, being primarily due to depolarized Mu.

A further experimental finding of this work suggests that hot Mu reactions are less significantly involved in high density fluids than may be generally believed, based on the fact that Mu is the only paramagnetic species observed in $ScCO_2$ over a very wide density range. If hot atom reactions of Mu* were to compete successfully with radiolysis reactions, we would have expected to observe the free radical MuOCO from addition reaction, particularly at higher densities—this has not been observed. On the other hand, CO_2, with its strong C═O bonds and large activation energies for reaction with H is a special case and thermalized Mu from collisions of Mu* with CO_2, contributing to P_{Mu}, cannot be ruled out.

The interplay between Mu and its intra-track reactions, due to radiation-induced species at high densities in CO_2, on a time scale of tens of ns, may be a key factor in understanding the nature of the radiation chemistry of other energetic heavy-charged particles in $ScCO_2$, notably from alpha-decay, in contrast to current studies (only) from electron pulse radiolysis. The dramatic increase in the lost fraction seen at high density in $ScCO_2$, caused by reactive transients (eqs 13−16), may have implications for corrosion in the materials of vessels used for radiation-induced polymerizations and nuclear waste management—due to the concentration and transport of transients that form during the radiolysis processes accompanying the thermalization of energetic ions, over a time scale of ~1−100 ns.

Acknowledgment. We thank Dr. Syd Kreitzman and the staff of the TRIUMF μSR facility for their technical support. Financial support from the Natural Sciences and Engineering Research Council of Canada is also greatly appreciated.

References and Notes

(1) Noyori, R., Ed. *Chem. Rev.* **1999**, *99*, 353−354.
(2) Eckert, C. A.; Knutson, B. L.; Debendetti P. G. *Nature* **1996**, *383*, 313−318.

(3) De Simone, J. M, Guanz, Z., Elsebernd, C. S. *Science* **1992**, *5072*, 945−947.
(4) Percival, P. W.; Ghandi, K.; Brodovitch, J.-C.; Addison-Jones, B.; McKenzie, I. *Phys. Chem. Chem. Phys*. **2000**, *2*, 4717−4720.
(5) Ghandi, K.; Brodovitch, J.-C.; Addison-Jones, B.; McCollum, B.; McKenzie, I.; Percival, P. W. *J. Am. Chem. Soc.* **2003**, *125*, 9594−9596.
(6) Batchelor, S. N.; Henningsen, B.; Fischer, H. *J. Phys. Chem. A* **1997**, *101*, 2969−2972.
(7) Gawenis, J. S.; Kauffman, J. F.; Jurisson, S. S. *Anal. Chem*. **2001**, *73*, 2022−2026.
(8) Iso, S., et al. *Prog. Nucl. Energy* **2000**, *37*, 423−428.
(9) Clifford, A. A.; Zhu, S.; Smart, N. G.; Lin, Y.; Wai, C. M.; Yoshida, Z.; Meguro, Y.; Schuichi, I. *J. Nucl. Sci. Tech.* **2001**, *38*, 433−438.
(10) Dostal, V.; Hejzlar, P.; Driscoll, M. J.; Todreas, N. E., ICONE10-22192, 10th International Conference on Nuclear Engineering, Arlington, Virginia, April 14−18, 2002.
(11) Dimitrijevic, N. M.; Bartels, D. M.; Jonah, C. D.; Takahashi, K. *Chem. Phys. Lett*. **1999**, *309*, 61−65.
(12) Dimitrijevic, N. M.; Takahashi, K.; Bartels, D. M.; Jonah, C. D.; Trifunac, A. D. *J. Phys. Chem. A* **2000**, *104*, 568−573.
(13) Shkrob, A.; Sauer, M. C. *J. Phys. Chem. B* **2001**, *105*, 7027−7032; ibid, *105*, 4520−4530.
(14) Shkrob, A.; Sauer, M. C.; Jonah, C. D.; Takahashi, K. *J. Phys. Chem. A* **2002**, *106*, 11855−11870.
(15) Takahashi, K.; Sawamura, S.; Dimitrijevic, N. M.; Bartels, D. M.; Jonah, C. D. *J. Phys. Chem. A* **2002**, *106*, 108−115.
(16) Mozumder, A. *Fundamentals of Radiation Chemistry*; Academic Press: London, 1999.
(17) Pimblott, S. M.; LaVerne, J. A. *J. Phys. Chem. A*. **1997**, *101* 5828−5838.
(18) Percival, P. W.; Fischer, H.; Camani, M.; Gygax, F. N.; Rüegg, W.; Schenck, A.; Schilling, H.; Graf, H. *Chem. Phys. Lett*. **1976**, *39*, 333−335.
(19) Percival, P. W.; Roduner, E.; Fischer, H. *Chem. Phys*. **1978**, *32*, 353−367.
(20) Walker, D. C. *Muon and Muonium Chemistry*; Cambridge University Press: Cambridge, 1983.
(21) Miyake, Y.; Tabata, Y.; Ito, Y.; Nishiyama, K.; Nagamine, K. *Radiat. Phys. Chem*. **1986**, *28*, 99−105.
(22) Mogensen, O. E.; Percival, P. W. *Radiat. Phys. Chem*. **1986**, *28*, 85−89.
(23) Leung, S. K.; Brodovitch, J. C.; Percival, P. W.; Yu, D.; Newman, K. E. *Chem. Phys*. **1988**, *121*, 393−403.
(24) Percival, P. W. *Hyperfine Interact*. **1990**, *65*, 901−911.
(25) Percival, P. W.; Brodovitch, J. C.; Ghandi, K.; Addison-Jones, B.; Schüth, J.; Bartels, D. M. *Phys. Chem. Chem. Phys*. **1999**, *1*, 4999−5004.
(26) Salmon, G. A. *Phys. B* **2003**, *326*, 46−50.
(27) Jonah, C. D. *Radiat. Res.* **1995**, *144*, 141−147.
(28) Roduner, E.; Brinkman, G. A.; Lowrier, W. F. *Chem. Phys*. **1984**, *88*, 143−153.
(29) Walker, D. C.; Karolczak, S.; Porter, G. B.; Gillis, H. A. *J. Chem. Phys*. **2003**, *81*, 199−203.
(30) Walker, D. C.; Karolczak, S.; Gillis, H. A.; Porter, G. B. *Can. J. Chem.* **2003**, *81*, 3233−3236.
(31) Eshchenko, D. G.; Storchak, V.; Brewer, J. H.; Morris, G. D.; Cox, S. F. J. *Phys. Rev. B* **2002**, *66*, 35105−35112.
(32) Siebbeles, L. D. A.; Pimblott, S. M.; Cox, S. F. J. *J. Chem. Phys*. **1999**, *111*, 7493−7500.
(33) Kempton, J. R.; Senba, M.; Arseneau, D. J.; Gonzalez, A. C.; Garner, D. M.; Pan, J. J.; Fleming, D. G.; Percival, P. W.; Brodovitch, J. C.; Leung, S. K. *J. Chem. Phys*. **1991**, *94*, 1046−1059.
(34) Eshchenko, D. G.; Storchak, V.; Brewer, J. H.; Cottrell, S. P.; Cox, S. F. J.; Karlsson, E.; Waeppling, R. *J. Low Temp. Phys*. **2001**, *27*, 854−857.
(35) Ghandi, K.; Brodovitch, J.-C.; Addison-Jones, Kecman, S. B.; McKenzie, I.; Percival, P. W. *Phys. B* **2003**, *326*, 76−80.
(36) Ghandi, K.; Brodovitch, J.-C.; Addison-Jones, B.; Percival, P. W.; Schüth, J. *Phys. B* **1999**, *289*, 476−481.
(37) Ghandi, K.; Brodovitch, J.-C.; Addison-Jones, B.; Percival, P. W.; Schüth, J. *Phys. Chem. Chem. Phys.* **2002**, *4*, 586−595.
(38) Kempton, J. R.; Senba, M.; Arseneau, D. J.; Gonzalez, A. C.; Tempelmann A.; Garner, D. M.; Fleming, D. G. *Hyperfine Int*. **1990**, *65*, 801−805.
(39) Kestin, J.; Sengers; J. V.; Kamgar-Parsi; B.; Levelt Sengers, J. M. H. *J. Phys. Chem. Ref. Data* **1984**, *13*, 175−183.
(40) Vesovic, V.; Wakeham, W. A.; Olchowy, G. A.; Sengers, J. V.; Watson, J. T. R.; Millat, J. *J. Phys. Chem. Ref. Data* **1990**, *19*, 763−808.
(41) Fleming, D. G.; Senba, M. in *Perspectives in Meson Science*; Yamazaki, T., Nakai, K., Nagamine, K., Eds.; North-Holland Press: Basel, Switzerland, 1992; p 219.
(42) Schenck, A. *Muon Spin Rotation Spectroscopy: Principles and Applications in Solid State Physics*; A. Hilger: Bristol, 1985.
(43) Cox, S. F. J. *Solid State Nucl. Magn. Res*. **1998**, *11*, 103−121.
(44) Roduner, E. *The Positive Muon as a Probe in Free Radical Chemistry*; Lecture Notes in Chemistry; Springer-Verlag: Berlin, 1988; Vol. 49.
(45) Roduner, E. *Chem. Soc. Rev*. **1993**, *22*, 337−346.
(46) Span, R.; Wagner, W. *J. Phys. Chem. Ref. Data* **1996**, *25*, 1509−1596.
(47) Inokuti, M. *Rev. Mod. Phys.* **1971**, *43*, 297−347.
(48) Fleming, D. G.; Mikula, R. J.; Garner, D. M. *Phys. Rev. A*. **1982**, *26*, 2527−2530.
(49) Senba, M. *J. Phys. B: At. Mol. Opt. Phys*. **1998**, *31*, 5233−5260.
(50) Senba, M.; Arseneau, D. J.; Gonzalez, A. C.; Kempton, J. R.; Pan, J. J.; Fleming, D. G. *Hyp. Int*. **1990**, *65*, 793−801.
(51) Arseneau, D. J.; Garner, D. M.; Senba, M.; Fleming, D. G. *J. Phys. Chem.* **1984**, *88*, 3688−3694.
(52) LaVerne, J. A.; Schuler, R. H. *J. Phys. Chem.* **1982**, *86*, 2282−2284.
(53) Sauer, M. C., Jr.; Jonah, C. D.; Schmidt, K. H.; Naleway, C. A. *Radiat. Res*. **1983**, *93*, 40−50.
(54) Elliot, A. J.; Chenier, M. P.; Ouellette, D. C.; Koslowsky, V. T. *J. Phys. Chem.* **1996**, *100*, 9014−9020.
(55) Cobut, V.; Frongillo, Y.; Patau, J. P.; Goulet, T.; Fraser, M−J.; Jay-Gerin, J.-P. *Radiat. Phys. Chem.* **1998**, *51*, 229−243.
(56) LaVerne, J. *Radiat. Res.* **2000**, *153*, 487−496.
(57) Fleming, D. G. *Radiat. Phys. Chem.* **1986**, *28*, 115−126.
(58) Senba, M.; Fleming, D. G.; Arseneau, D. J.; Mayne, H. R. J. *Chem. Phys*. **2000**, *112*, 9390−9403.
(59) Kempton, J. R.; Arseneau, D. J.; Fleming, D. G.; Senba, M.; Gonzalez, A. C.; Pan, J. J.; Garner, D. M. *J. Phys. Chem.* **1991**, *95*, 7338−7344.
(60) Percival, P. W.; Brodovitch, J. C.; Arseneau, D. J.; Senba, M.; Fleming, D. G. *Phys. B* **2003**, *326*, 72−75.
(61) Fleming, D. G.; Mikula, R. J.; Senba, M.; Garner, D. M.; Arseneau, D. J. *Chem. Phys*. **1983**, *82*, 75−86.
(62) Arseneau, D. J.; Fleming, D. G.; Senba, M.; Reid, I. D.; Garner, D. M. *Can. J. Chem*. **1988**, *66*, 2018−2024.
(63) Eshchenko, D. G.; Storchak, V.; Brewer, J. H.; Cottrell, S. P.; Cox, S. F. J. *J. Low Temp. Phys*. **2003**, *29*, 185−195.
(64) Storchak, V.; Brewer, J. H.; Eshchenko, D. G. *Appl. Magn. Res*. **1997**, *1*−*2*, 15−24.
(65) Ghandi, K.; Arseneau, D. J.; Bridges, M. D.; Fleming, D. G.; Patey, G.; Wang A. Y.; Zahariev F., work in progress.
(66) Laria, D.; Martí, J.; Guardia, E. *J. Am. Chem. Soc.* **2004**, *126*, 2125−2134.
(67) Martí, J.; Andrés, J. L.; Bertráni J.; Duran, M. *Mol. Phys.* **1993**, *80*, 625−633.
(68) Agmon, N. *J. Phys. Chem.* **1996**, *100*, 1072−1080.
(69) Boero, M.; Terakura, K.; Ikeshoji, T.; Chee Chin, L.; Parrinello, M. *Phys. Rev. Lett.* **2000**, *85*, 3245−3248.
(70) Duncan, T. V.; Miller, C. E. *J. Chem. Phys*. **2000**, *113*, 5138−5140.
(71) Troya, D.; Lakin, M. J.; Schatz, G. C.; Harding, L. B.; Gonzalez, M. *J. Phys. Chem. B* **2002**, *106*, 8148−8160.
(72) Baer, S.; Fleming, D. G.; Arseneau, D. J.; Senba, M.; Gonzalez, A. C. *ACS Advances in Chemistry Series 502* **1992**, 111−137.
(73) Scherer, N. F.; Khundkar, L. R.; Bernstein, R. B.; Zewail, A. H. *J. Chem. Phys.* **1987**, *87*, 1451−1453.
(74) Fushitani, M.; Shida, T.; Rasanen, M. *J. Phys. Chem. A* **2000**, *104*, 3635−3641.
(75) Golden, D. M.; Smith, G. P.; McEwen, A. B.; Yu, C. L.; Eiteneer, B.; Frenklach, M.; Vaghjiani, G. L.; Ravishankara, A. R. Tully, F. P. *J. Phys. Chem. A* **1998**, *102*, 8598−8606.
(76) Brouard, M.; Hughes, D. W.; Kalogerakis, K. S.; Simons, J. P. *J. Phys. Chem. A* **1998**, *102*, 9559−9564.
(77) Reid, I. D.; Cox, S. F. J.; Jayasooriya, U. A.; Hopkins, G. A. *Magn. Reson. Chem*. **2000**, *38*, 3−8.
(78) Fukuchi, T. *Jpn. J. Appl. Phys.* **1996**, *35*, 1977−1982.
(79) Becker, D.; Lavere, T.; Sevilla, M. D. *Radiat. Res.* **1994**, *140*, 123−129.
(80) Brown, J. M.; Schubert, J. E. *J. Mol. Spec*. **1982**, *95*, 194−212.
(81) Jacox, M. E. *J. Chem. Phys.* **1988**, *88*, 4598−4607.
(82) Ruscic, B.; Schwarz, M.; Berkowitz, J. *J. Chem. Phys.* **1989**, *91*, 6780−6785.
(83) Paraskevopoulos, G.; Irwin, R. S. *J. Chem. Phys*. **1984**, *80*, 259−266.
(84) Miyoshi, A.; Matsui, H.; Washida, N. *J. Chem. Phys*. **1993**, *100*, 3532−3539.
(85) Marques, J. M. C.; Llanio-Trujillo, J. L.; Varandas, A. J. C. *PCCP* **2000**, *16*, 3583−3589.
(86) Atherton, N. M. *Principles Of Electron Spin Resonance*; Prentice Hall: New York, 1993.
(87) Weltner, W. *Magnetic Atoms and Molecules*; Dover Publications: Mineola, NY, 1989.
(88) Batchelor, S. N. *J. Chem. Phys.* **1998**, *102*, 615−619.

(89) Fleming, D. G.; Pan, J. J.; Senba, M.; Arseneau, D. J.; Kiefl, R. F.; Shelley, M. Y.; Cox, S. F. J.; Percival, P. W.; Brodovitch, J. C. *J. Chem. Phys*. **1996**, *105*, 7517−7535.
(90) Sears, T.; Radford, H. E.; Moore, M. A. *J. Chem. Phys*. **1993**, *98*, 6624−6631.
(91) Fenghour, A.; Wakeham, W. A.; Vesovic, V. *J. Phys. Chem. Ref. Data* **1998**, *27*, 31−44.
(92) Senba, M. *Phys. Can.* **1997**, *53*, 305−312.
(93) Senba, M.; Fleming, D. G.; Arseneau, D. J.; Garner, D. M.; Reid, I. D. *Phys. Rev. A* **1989**, *39*, 3871−3883.
(94) Friend, D. G.; Ingham, H.; Ely, J. F. *J. Phys. Chem. Ref. Data* **1991**, *20*, 275−347.
(95) Barnett, R. N.; Landman, U.; Nitzan, A. *J. Chem. Phys.* **1990**, *11*, 8187−8195.
(96) Gee, N.; Senaanayake, P. C.; Freeman, G. R. *J. Chem. Phys.* **1988**, *6*, 3710−3717.